Available online at www.sciencedirect.com
ScienceDirect
Trans. Nonferrous Met. Soc. China 32(2022) 3596−3609
Transactions of Nonferrous Metals Society of China
www.tnmsc.cn

Effect of bias voltage on microstructure, mechanical and tribological properties of TiAlN coatings

Hong-shuai CAO[1,2], Fu-jia LIU[1,2], Hao LI[1,2], Wen-zhong LUO[1,2], Fu-gang QI[1,2], Li-wei LU[3], Nie ZHAO[1,2], Xiao-ping OUYANG[1,2]

1. School of Materials Science and Engineering, Xiangtan University, Xiangtan 411105, China;
2. Key Laboratory of Low Dimensional Materials and Application Technology of Ministry of Education, Xiangtan University, Xiangtan 411105, China;
3. Hunan Provincial Key Laboratory of High Efficiency and Precision Machining of Difficult-to-Cut Material, Hunan University of Science and Technology, Xiangtan 411201, China

Received 3 September 2021; accepted 28 March 2022

Abstract: TiAlN multilayer coatings composed of TiAl and TiAlN layers were deposited on ZL109 alloys using filtered cathodic vacuum arc (FCVA) technology. The effect of bias voltage on the microstructure and properties of the coating was systematically studied. The results show that the coating exhibits a multi-phase structure dominated by TiAlN phase. As the bias voltage increases, the orientation of TiAlN changes from (200) plane to (111) plane due to the increase of atomic mobility and lattice distortion. The hardness, elastic modulus and adhesion of the coating show the same trend of change, that is, first increase and then decrease. When the bias voltage is 75 V, the coating exhibits the highest hardness (~30.3 GPa), elastic modulus (~229.1 GPa), adhesion (HF 2) and the lowest wear rate (~4.44×10^{-5} $mm^3/(N\cdot m)$). Compared with bare ZL109 alloy, the mechanical and tribological properties of TiAlN coated alloy surface can effectively be improved.

Key words: TiAlN coatings; filtered cathodic vacuum arc; bias voltage; microstructure; mechanical properties; wear

1 Introduction

Aluminum (Al) alloys have the advantages of low density and high specific strength, and are widely applied in automotive, aerospace and aviation industries [1,2]. Especially, in the automotive industry, Al alloy pistons have attracted more and more attention to achieve lightweight engines that meet stricter fuel economy and emission standards. However, the poor mechanical performance and tribological behaviors of Al alloys (i.e., low hardness and load-bearing capacity, high friction coefficient and wear rate) may lead to friction loss, ablation, cracking and jamming damage, which limits the development of pistons [3,4]. Therefore, it has become the focus of research on Al alloy pistons to effectively improve the surface hardness and wear resistance without changing its own performance.

TiAlN ceramic coating may become one of the most promising surface protection materials for Al alloys due to its unique properties [5,6]. WU et al [7] reported that the TiAlN coating exhibited low coefficient of friction and high hardness. Moreover, the TiAlN coating showed higher hardness (about 34 GPa) due to solid solution strengthening compared to binary TiN and ZrN (approximately 27 and 21 GPa) [8,9]. In addition, BADINI et al [10] found that TiAlN coatings can also significantly

Hong-shuai CAO and Fu-jia LIU contributed equally to this work
Corresponding author: Fu-gang QI, Tel: +86-731-58298119, E-mail: qifugang@xtu.edu.cn
DOI: 10.1016/S1003-6326(22)66042-4

improve oxidation resistance by affecting the diffusion phenomenon in cyclic oxidation tests, thereby providing oxidation protection for intermetallic alloys. However, in these studies, most of the TiAlN coatings were deposited on the surface of hard substrates, while there were few reports on TiAlN coatings on soft substrates. In general, the mismatch of the thermal expansion coefficients between the Al alloy substrate and the hard TiAlN coating will generate high thermal stress at the interface, resulting in adhesion failure. In addition, the increase in defects also leads to an increase in internal stress during the coating growth process. Therefore, the poor adhesion strength caused by high residual stress is the main challenge for the application of TiAlN coatings on Al alloy surfaces.

Multilayer structure design is an effective way to release residual stress during coating deposition. At present, the intermediate layers studied mainly include Ti [11], TiAl [12], TiN [13], AlN [14] and ZrN [15], etc. As a transition zone, the intermediate layer can cause a continuous compositional change that effectively matches the compatibility of the physical and chemical properties between the coating and the substrate. In addition, the ductile metal as an intermediate layer can not only reduce the residual stress, but also reduce the porosity and increase the toughness of the coating. Furthermore, interfacial and grain boundary effects can also improve the performance of the coating.

In recent years, the addition of ductile Ti and TiAl metal layers in TiAlN coatings has attracted increasing attention due to the high affinity of Ti for TiAlN and the excellent oxidation resistance of Al. ZHAO et al [16] prepared Ti/TiAlN gradient coatings on 2024 Al/SiC_p substrates by continuously increasing the N_2 flow rate during deposition, and found that the internal stress of the coating is uniformly distributed along the growth direction, rather than concentrated at the interface between the coating and the substrate. The uniform distribution of stress in the Ti/TiAlN gradient coating can effectively eliminate the stress concentration at the interface to a certain extent, thereby avoiding coating delamination and improving adhesion strength. Additionally, SHUGUROV and KAZACHENOK [12] reported that the TiAlN/TiAl multilayer coating exhibited a higher critical load and a three-fold reduction in wear rate compared to the monolayer TiAlN coating due to enhanced toughness and adhesion. The toughening mechanism of the multilayer structure is that crack deflection at the interlayer interface can provide additional dissipative strain energy, effectively compensating for the increase in dissipative work caused by crack propagation in the ductile metal layer. Furthermore, OSTROVSKAYA et al [17] found that the two-layer TiAl/TiAlN coating showed excellent oxidation resistance in thermal cycling experiments up to 1000 °C. Obviously, TiAlN multilayer coatings with high hardness, high adhesion strength, excellent wear resistance and oxidation resistance have great application potential in Al alloy pistons.

In this work, TiAl/TiAlN multilayer coatings were deposited on Al alloys by filtered cathodic vacuum arc (FCVA) technology with TiAl alloy as the target material and N_2 as the reactive gas. The effect of bias voltage on the microstructure, mechanical and tribological properties of TiAlN coatings was investigated. The systematic study of the preparation, microstructure and performance of TiAlN coating on Al alloy has certain significance for the surface protection of pistons. In addition, it has certain practical value for expanding the application of hard TiAlN coatings.

2 Experimental

TiAlN coatings were prepared on ZL109 alloy substrates with dimensions of 20 mm × 20 mm × 5 mm using FCVA equipment, as shown in Fig. 1. Before the experiment, the substrate was ground and mirror-polished, and then ultrasonically cleaned

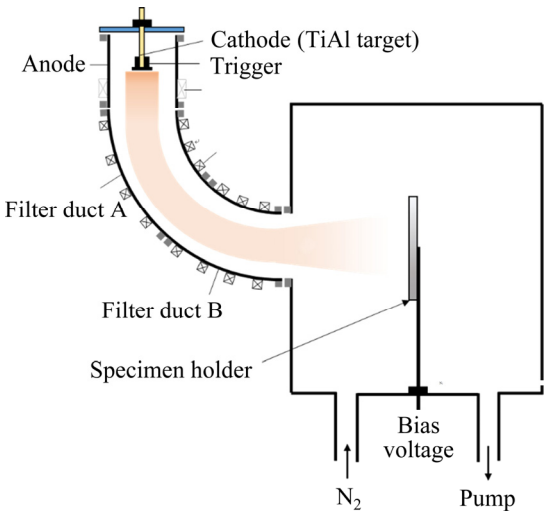

Fig. 1 Schematic diagram of FCVA deposition system

in acetone and alcohol for 15 min. Subsequently, the substrate was placed on the rotating holder with a distance of 15 cm from the outlet of filter duct. The coating preparation was carried out in low vacuum with a base pressure lower than 3.5×10^{-3} Pa to reduce the influence of oxygen. A TiAl alloy target with a molar ratio of 30:70, a purity of 99.99% and a diameter of 100 mm was used as the cathode. The cathodic arc was triggered at a current of 90 A to generate the plasma. The filter ducts were used to effectively filter unwanted neutral atoms and macroparticles under the action of electromagnetic fields. N_2 with a purity of 99.99% was introduced as the nitrogen source.

The schematic diagram of the film structure of the TiAlN coating is shown in Fig. 2, and the deposition process includes the following four steps. Firstly, prior to deposition, the substrate was further cleaned and etched by plasma sputtering. During this process, the bias voltage was adjusted from 900 to 400 V by reducing 100 V per 30 s. Secondly, a TiAl transition layer was deposited at a bias voltage of 100 V. Then, a compositional gradient zone was prepared by introducing N_2 and increasing the flow rate to 70 mL/min at a rate of 5 mL/min per 30 s. Finally, a TiAlN layer was deposited by maintaining a flow rate of 70 mL/min for 40 min. The experiment was carried out at room temperature without other intentional heating. Additionally, the sample holder was maintained at a rotation speed of 5 r/min for uniform deposition. To investigate the effect of bias voltage on the structure and properties of TiAlN coatings, the bias voltage was set at 50, 75 and 100 V during the deposition of TiAlN layers. The detailed deposition parameters of TiAl/TiAlN coatings are listed in Table 1.

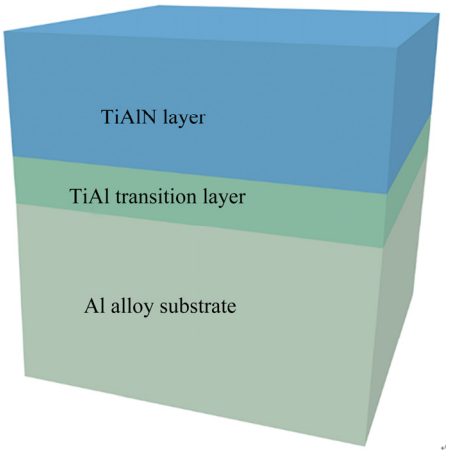

Fig. 2 Schematic diagram of TiAlN coating film structure

Table 1 Deposition parameters of TiAl/TiAlN coatings

Deposition parameter	TiAl transition layer	TiAlN coating
Target	$Ti_{30}Al_{70}$	$Ti_{30}Al_{70}$
Cathode current/A	90	90
Positive bias voltage/V	24	24
Filter coil A current/A	2.5	2.5
Filter coil B current/A	3.2	3.2
Bias voltage duty cycle/%	90	90
Substrate holder rotation speed/(r·min^{-1})	5	5
Deposition temperature/°C	25	25
N_2 flow rate/(mL·min^{-1})	−	70
Bias voltage/V	100	50, 75, 100
Deposition time/min	15	40

Scanning electron microscope (SEM, JSM−7800F) was utilized to characterize the surface and cross-sectional morphologies of the coatings.

Three-dimensional confocal laser scanning microscopy (CLSM) was also used to analyze surface morphology and wear track. An energy dispersive spectrometer (EDS, X−Max20) was applied to detecting the composition of the coating. The phase structure was determined using X-ray diffraction (XRD, Cu K_α radiation, λ=1.5406 Å) in the 2θ range from 20° to 85° at a scanning step of 0.02°. In addition, X-ray photoelectron spectroscope (XPS, ECSALAB 250XI) was used to determine the binding energy of the coatings under monochromatic Al K_α irradiation with a pass energy of 30 eV and an energy step of 0.05 eV.

The mechanical properties of the coatings were investigated by a nanoindentation device (TI−900, Hysitron) in load-controlled mode under a penetration load of 20 mN. A Poisson's ratio of 0.18 was assumed to calculate the elastic modulus of TiAlN [18]. The tribological performance was investigated by ball-on-disk tribometer (UMT−2) using a 440C stainless-steel ball with 10 mm in diameter. The experimental parameters were set to a constant linear velocity of 0.12 m/s, a sliding time of 1200 s and a normal load of 3 N. In addition, the CLSM was applied to assessing the wear volume through the cross-section area of the wear track, and the wear rate was calculated by the following formula:

$$W=V/(P\cdot L) \quad (1)$$

where W, V, P and L are wear rate, wear volume, normal load and sliding distance, respectively. Furthermore, Rockwell HRC indentation was performed to evaluate the adhesion strength at a maximum force of 150 kg. Optical microscopy (Olympus BX53M) was used to determine the morphology of the indentation.

3 Results and discussion

3.1 Composition and microstructure of TiAlN coating

The chemical composition of TiAlN coatings with different bias voltages is detected by EDS. As shown in Fig. 3, the Ti, Al, N and C elements can be distinguished in the coating. The reason for the existence of C may be caused by impurities adsorbed on the coating surface. As the bias voltage increases from 50 to 100 V, the Ti content increases from 22.13 to 23.18 at.%, while the Al content decreases from 24.65 to 22.68 at.%. Moreover, the N content is almost maintained at about 51.67 at.%. The variation of Ti and Al contents is related to the charge state distribution of ions in the ion flux. The average charge states ($\bar{Q}_p$) of Ti and Al are +2.1 and +1.7, respectively [19]. During coating deposition, Ti ions with higher charge state distribution bombard the surface with higher energy and penetrate deeper into the coating under the action of the bias voltage. Therefore, the Ti content increases with increasing bias voltage. In contrast, Al ions with lower charge state distribution are more likely to reverse sputtering phenomenon. In addition, lighter Al atoms are preferentially sputtered over Ti atoms, resulting in a more obvious sputtering effect [20]. Therefore, the preferential reverse sputtering of Al leads to its content loss due to the increase of the sputtering energy with the increase of the bias voltage.

Moreover, it can also be found that the molar ratio of Al to Ti in the coating is about 1:1, which is lower than that of the $Ti_{30}Al_{70}$ target. The reason for this phenomenon can be explained by the different ionization degrees of Al and Ti. The ionization degree of Al vapor (50%) is lower than that of Ti vapor (80%). Thus, Ti ions are preferentially attracted to the substrate surface under the action of bias voltage, resulting in a lower Al/Ti ratio in the coating [21]. In addition, Al ions with lower average charge state show stronger diffusion to the outside of the beamline under the same electric field. This also leads to the loss of Al during transmission. In summary, the reduction of Al content in the coating caused by the above hybrid effect is the reason why the Al/Ti ratio deviates from the value of the alloy target.

Figure 4 shows the XRD patterns of TiAlN coatings with various bias voltages. Since the penetration depth of X-rays is greater than the coating thickness, the XRD pattern presents the main diffraction peaks of the coating as well as a few substrate peaks. Diffraction peaks located at 2θ values of approximately 38.39°, 44.68°, 65.06°, 78.18° and 82.35° can be identified as (111), (200), (220), (311) and (222) planes of face-centered cubic (fcc) TiAlN (PDF #37-1140), respectively. Peaks around 35.42° and 36.89° could be associated with the (111) plane of AlN (PDF #25-1495) and cubic TiN (PDF #38-1420), respectively. Furthermore, it can be observed that AlN and TiN peak intensities are much lower than those of TiAlN, indicating poor crystallinity. According to the literature [22],

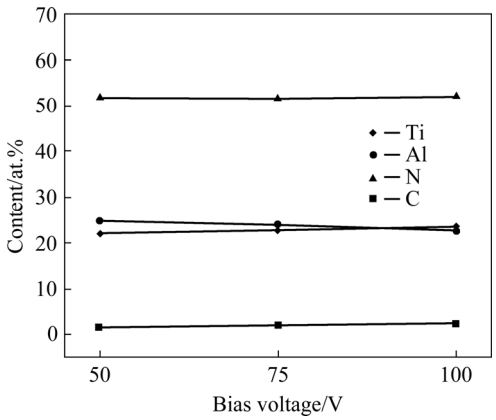

Fig. 3 Chemical composition of TiAlN coatings with different bias voltages

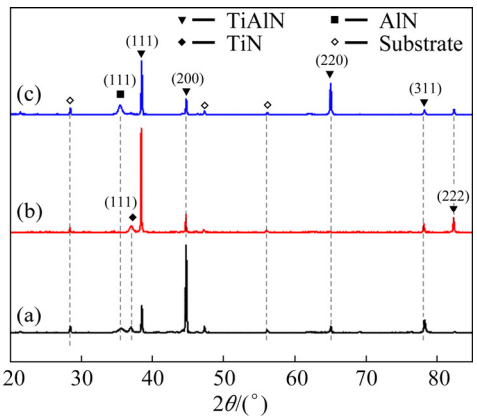

Fig. 4 XRD patterns of TiAlN coatings with different bias voltages: (a) 50 V; (b) 75 V; (c) 100 V

the chemical formation energies of TiN and AlN are −305.6 and −241.6 kJ/mol. Cubic TiN is formed preferentially in the Ti, Al and N molecular system. However, Al atoms can replace part of the Ti atoms in TiN to form TiAlN compounds, and TiAlN still maintains the *B*1-NaCl cubic crystal structure. Therefore, the diffraction peak intensities of AlN and TiN are relatively low, and only (111) plane is apparent. In addition, the intensity of the AlN diffraction peak decreases or disappears with increasing bias voltage, and the structure of the coating is dominated by TiAlN phase.

The orientation of the TiAlN diffraction peaks strongly depends on the bias voltage. When the bias voltage is 50 V, TiAlN (200) is obviously the preferred growth orientation compared to the (111) diffraction peak. According to the principle of minimum energy, the grain orientation tends to grow along the plane with the lowest free energy determined by the surface and strain energy [23,24]. Due to the difference in atomic radius, the substitution of Al for Ti causes lattice distortion, thereby increasing the strain energy. By interrupting the growth of the TiAl layer, the strain energy can be converted into the interface energy between the TiAl and the TiAlN layers. Here, the (200) plane has a lower strain energy density than the (111) plane, which can provide a driving force for the grain growth [25,26]. Therefore, the coating shows a preferred orientation of TiAlN (200) plane. However, as the bias voltage increases from 50 to 75 V, the orientation of TiAlN changes from (200) plane to (111) plane, and the (220) diffraction peak disappears. The preferred orientation of TiAlN can be strongly affected by ion bombardment [27,28]. With increasing the bias voltage, the higher ion bombardment energy leads to higher energy of atoms adsorbed on the substrate, resulting in lattice distortion and increased atomic mobility. This can increase the strain energy and promote the growth of the coating along the (111) plane. When the bias voltage is further increased to 100 V, the intensity of TiAlN (111) orientation decreases slightly, while the (220) diffraction peak occurs for the coating. Selective etching or reverse sputtering of ions under high bias voltage may also affect the growth orientation of TiAlN during deposition. The preferred orientation change of TiAlN with increasing bias voltage is similar to the results reported in the literature [29].

As shown in Fig. 5, the similar shapes between each other in the Ti 2p, Al 2p, and N 1s spectra can be observed in XPS spectra of TiAlN coatings with different bias voltages. In Fig. 5(a), Ti 2p spectra exhibit two typical doublets at 453−460 and 460−467 eV, which are associated with the Ti $2p_{3/2}$ and Ti $2p_{1/2}$ states, respectively. Furthermore, all Ti 2p spectra can be further fitted into six Gaussian peaks. The Ti $2p_{3/2}$ and Ti $2p_{1/2}$ peaks centered at (455.1±0.2) and (460.5±0.2) eV are related to the Ti—Al—N bonds [30,31], corresponding to TiAlN compounds. The intensity of the Ti—Al—N peak (about 545.1 eV) weakens with increasing bias voltage, which may be due to the lattice distortion. Moreover, the peaks at (456.7±0.2) and (462.4±0.2) eV are related to Ti $2p_{3/2}$ and Ti $2p_{1/2}$ peaks of Ti — O — N bonds (TiN_xO_y compounds) [32], respectively. The binding energies of (458.3±0.3) and (464.2±0.2) eV belong to the Ti—O bonds in TiO_2 [33]. Compared with N, Ti has a higher affinity to O atoms. Therefore, Ti easily combines with trace oxygen remaining in the chamber and oxygen exposed to air to form titanium oxides.

Additionally, Al 2p spectra in Fig. 5(b) are decomposed into three main peaks at (73.5±0.1), (74.2±0.1) and (74.8±0.1) eV. Among them, the lowest value is lower than 74.5 eV of AlN and higher than 72.8 eV of metallic Al. This may be attributed to non-stoichiometric AlN_x compounds or ternary compounds [34,35]. According to the binding energy analysis of the Ti 2p spectra, the peak at 73.5 eV can be associated to Ti—Al—N bonds (TiAlN ternary compounds), which is also consistent with the report by RIZZO et al [36]. The medium binding energy value can be related to Al—N bonds in AlN, whereas the highest binding energy value corresponds to Al — O bonds in γ-Al_2O_3 [35]. Similarly, N 1s spectra can be fitted into three peaks, as shown in Fig. 5(c). These peaks are assigned to Ti — N bonds ((396.5±0.1) eV, TiN) [11], Al — N — Ti and N — Al bonds ((397.4±0.2) eV, TiAlN and AlN compounds) [36], and N_2 surface adsorbates (about 399.8 eV) [31]. Furthermore, Fig. 5(d) shows the C 1s spectra and the corresponding fitting results of TiAlN coatings with different bias voltages. The peaks at (284.8±0.1), (285.4±0.2) and (288.6±0.2) eV are attributed to C—C (or C—H), C—N and C═O bonds [37], which provide evidence that the presence of C is caused by adsorbed impurities.

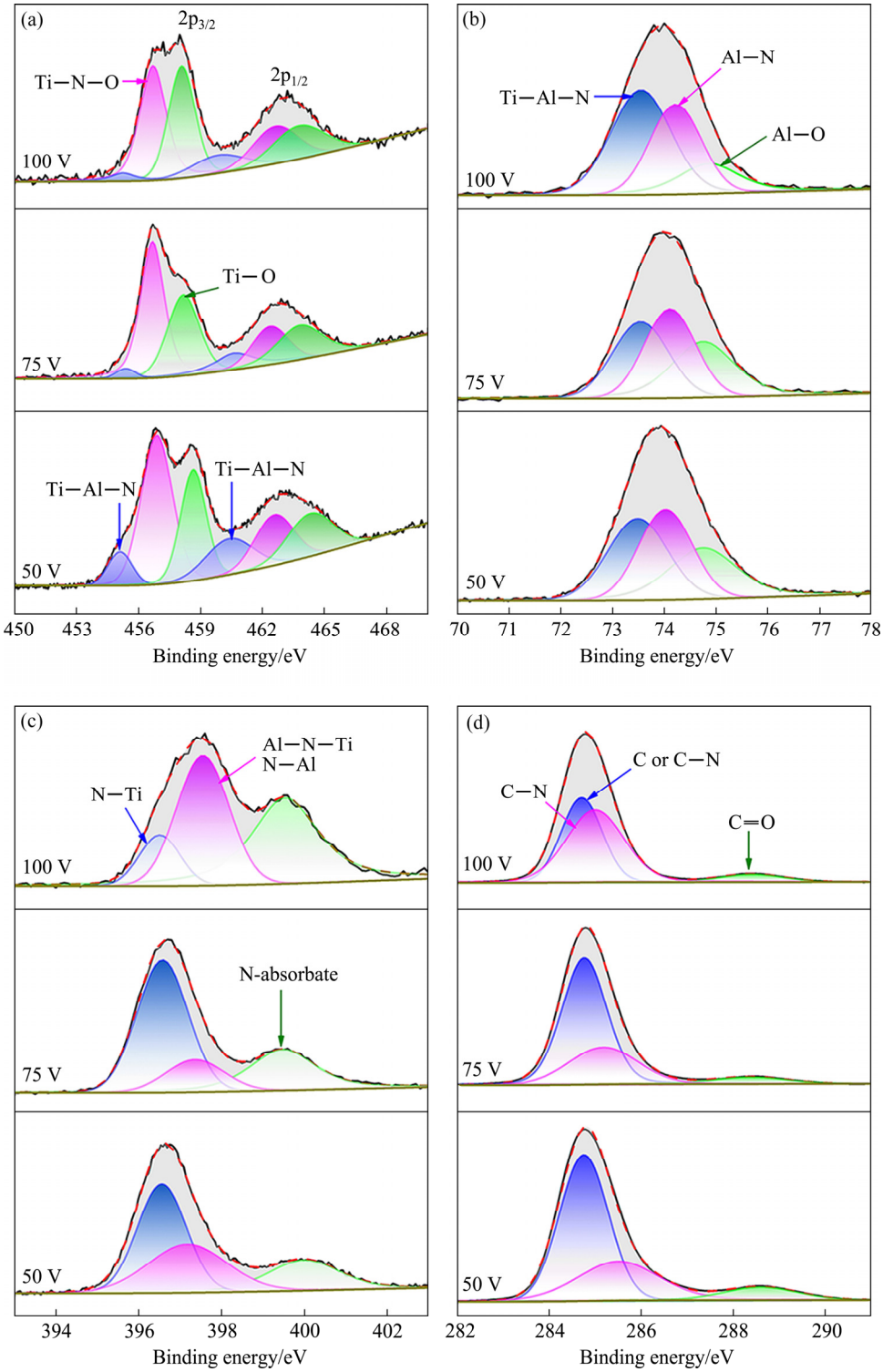

Fig. 5 Ti 2p (a), Al 2p (b), N 1s (c) and C 1s (d) XPS spectra of TiAlN coatings with different bias voltages

3.2 Surface and cross-sectional morphologies of TiAlN coating

The surface morphologies of TiAlN coatings with different bias voltages are shown in Fig. 6. The coating exhibits a continuous, uniform and dense structure without cracks. However, some macroparticles and micro-holes can be observed, which are considered to be characteristic of arc ion plating deposition [24]. By counting the number of macroparticles in the SEM images with similar magnification, it was found that the number of macroparticles has been effectively reduced by filtering electromagnetic fields compared to that reported in the literature [38]. The reasons for

formation of these macroparticles may come from the following aspects: (1) arc-emitted droplets appear on the TiAl target surface; (2) collision occurs when excess atoms or ions on the target interact with the substrate; (3) atoms or ions collide and accumulate on the substrate surface during deposition. Since the large droplets generated by the target material can be effectively filtered out by the electromagnetic field, the reason for the macroparticles in this study may be the collision and aggregation of lighter Al and Ti on the substrate surface.

The number of macroparticles on the surface of TiAlN coatings with different bias voltages is compared based on SEM images at the same magnification. The results show that as the bias voltage increases from 50 to 75 V, the number of macroparticles decreases due to the charge repulsion effect [39]. Macroparticles inevitably collide randomly with electrons, ions or neutral atoms as they move toward the substrate, collecting more electrons and becoming negatively charged. These electrons, ions or neutral atoms will also be absorbed by the macroparticles. Negatively-charged macroparticles can be filtered out by the electric field repulsion near substrate sheath, leading to a reduction in the number of macroparticles. However, when the bias voltage is further increased to 100 V, the surface quality of the coating deteriorates. This can be verified by the increase in the number of macroparticles and defects on the coating surface, as shown in Figs. 6(e, f). As the bias voltage increases, the internal ionization degree of the macroparticles increases, causing its transition from

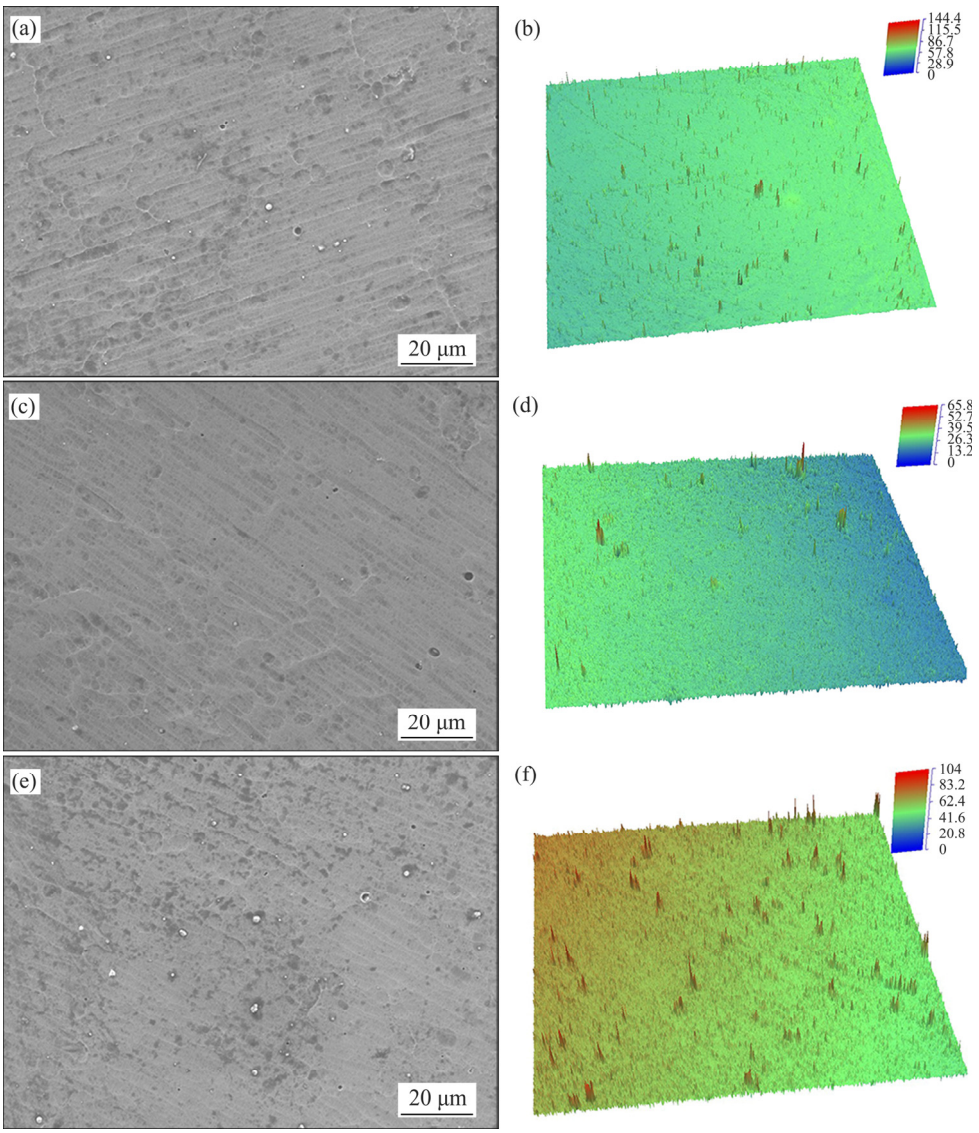

Fig. 6 SEM (a, c, e) and 3D optical (b, d, f) surface morphologies of TiAlN coatings deposited at different bias voltages: (a, b) 50 V; (c, d) 75 V; (e, f) 100 V

negative to positive charge, as reported by ZHANG et al [8]. The positively-charged macroparticles are attracted to the substrate surface, resulting in an increase in the number of macroparticles. The average roughness of the coatings with a bias voltage of 50, 75 and 100 V measured by the surface profiler is 0.032, 0.024 and 0.042 μm, respectively. Furthermore, the change of surface roughness with increasing bias voltage can be directly observed by the 3D surface morphology in Figs. 6(b, d, f).

Figure 7 shows the cross-sectional SEM morphologies and deposition rate of the coating. The cross-sections of the coatings with different bias voltages exhibit a uniform and compact structure with almost no cracks. Interface fringes can be apparently seen, implying a two-layer structure consisting of a TiAl transition layer and a TiAlN layer. Moreover, a blurry gradient zone with a thickness of about 200 nm is formed between the TiAl transition layer and the TiAlN layer, as shown in Fig. 7(b). As the coating grows from the gradient zone to the TiAlN layer, the structure transforms from columnar to fine equiaxed crystals, which is associated with a linear increase in the N_2 flow rate from 5 to 70 mL/min. Furthermore, the TiAl transition layer shows a similar thickness, around 1070 nm. The thickness of the TiAlN layer gradually decreases with the increase of the bias voltage. The high bias voltage leads to a decrease in the deposition rate of the TiAlN coating, as shown in Fig. 7(d). When the bias voltage is 100 V, the coating has the minimum thickness of approximately 3032 nm. This is because the reverse sputtering effect caused by ion bombardment at high bias voltage reduces the deposition rate of TiAlN coatings [20].

3.3 Adhesion and mechanical properties of TiAlN coating

The optical morphologies of the coating indentations with different bias voltages are shown in Fig. 8. Adhesion strength is determined by comparing the damage of the coating to a defined adhesion strength [40], where HF 1−4 grades correspond to sufficient adhesion, but both HF 5 and HF 6 indicate insufficient adhesion due to cracking and substrate visibility. When the coating is deposited at a bias voltage of 50 V, a large number of cracks and small separated parts can be observed around the indentation in Figs. 8(a, b), which can be defined as HF 3. As the bias voltage is increased to 75 V, the density of cracks is decreased significantly and the signs of separation around the

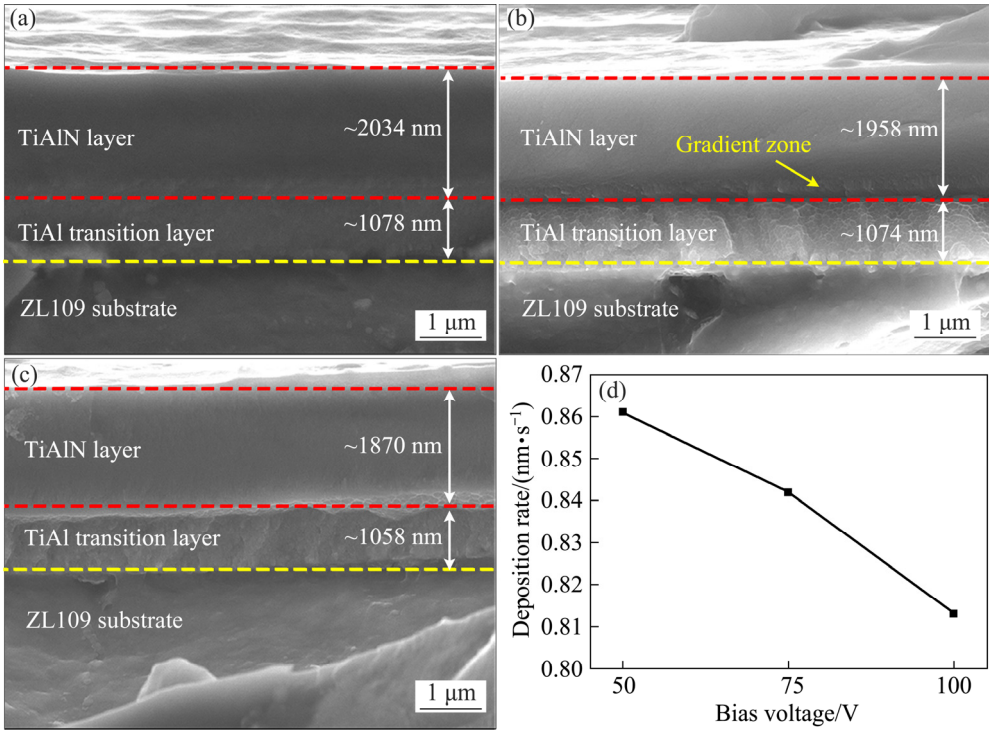

Fig. 7 Cross-sectional morphologies (a−c) and deposition rate (d) of TiAlN coatings deposited at different bias voltages: (a) 50 V; (b) 75 V; (c) 100 V

indentation are also diminished, as seen in Figs. 8(c, d). The adhesion strength is identified to be HF 2. However, the adhesion strength of the coating decreases at a bias voltage of 100 V due to the appearance of higher density cracks and larger detached areas in Figs. 8(e, f), which belongs to HF 3. In addition, there are some annular detachments around the indentation, but no typical radial cracks are observed. This phenomenon may be related to the high toughness of the TiAlN coating or the characteristics of the soft ZL109 alloy substrate. Overall, the TiAlN multilayer coating exhibits excellent adhesion strength (HF ≥ 3) to the ZL109 alloy substrate, which is beneficial to the practical application of the coating.

Figure 9 shows the mechanical properties of coatings with different bias voltages measured by nanoindentation. It can be found that the hardness and elastic modulus of the coating are closely related to the bias voltage. As the bias voltage increases from 50 to 75 V, the hardness of the TiAlN coating increases from 28.3 to 30.3 GPa. The vacancies caused by ion bombardment at higher bias voltage are more likely to be filled with newly-generated ions, resulting in increased packing density [41]. In addition, high bombardment energies favor grain refinement. According to the Hall−Petch formula, grain refinement is beneficial to improving the hardness of the coating [29,42]. Furthermore, an increase in the energy of the bombarding ions will also lead to an increase in the defect density owing to a decrease in surface mobility. Therefore, the greater lattice strain caused by the increase in defect density causes the residual

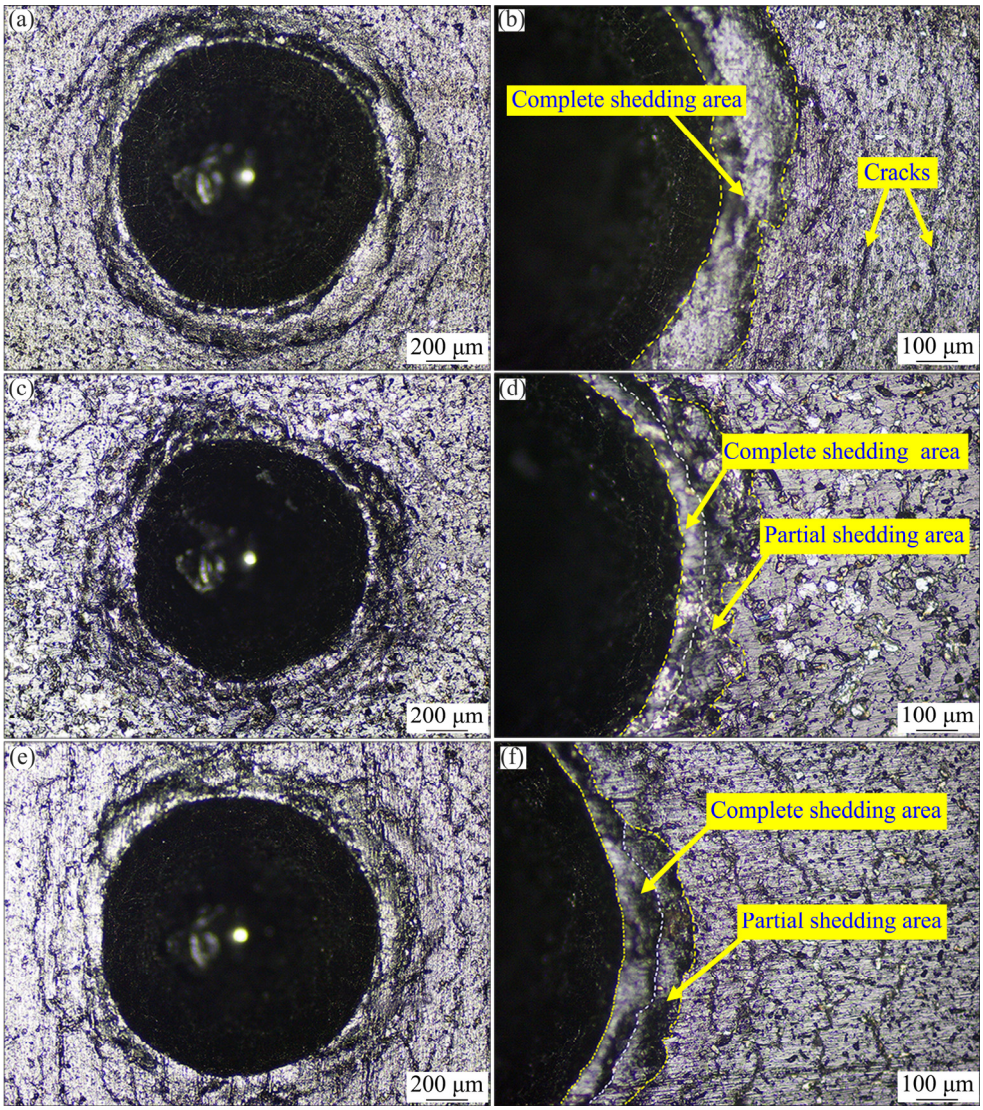

Fig. 8 Optical morphologies of Rockwell indentations of TiAlN coatings deposited at different bias voltages: (a, b) 50 V; (c, d) 75 V; (e, f) 100 V

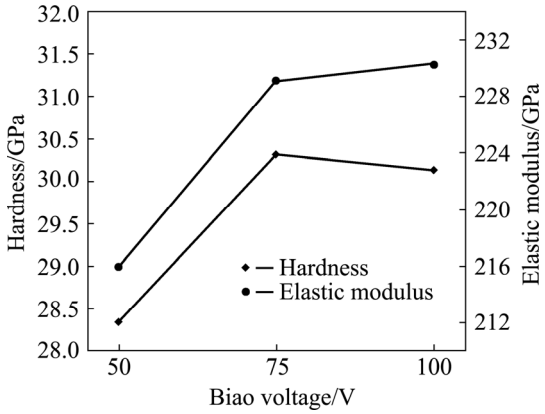

Fig. 9 Hardness and elastic modulus of TiAlN coatings with different bias voltages

compressive stress in the coating to increase [43], as evidenced by the transition of TiAlN orientation from the (200) plane to the (111) plane in Fig. 4. As the bias voltage increases from 50 to 75 V, the above-mentioned three factors of vacancy filling, grain refinement and residual stress increase the coating hardness.

However, as the bias voltage is further increased from 75 to 100 V, the hardness decreases slightly from 30.3 to 30.1 GPa. The effect of high temperature annealing effect caused by ion bombardment on the coating surface under high bias voltage is noteworthy. Due to the local heating of the coating, AlN in the fcc TiAlN host structure is separated to form a thermodynamically stable ω-AlN phase, which explains the existence of the AlN phase in the coating with a bias voltage of 100 V in Fig. 4. Moreover, the increase in atomic mobility under the effect of high temperature annealing leads to strain relaxation [28]. Once the strain relaxation is greater than the stress multiplication induced by ion bombardment, the residual compressive stress decreases. At the same time, the preferential sputtering of Al and the increase of lattice constant caused by the increase of bias voltage also result in the decrease of hardness [8]. The above factors can explain the decrease of coating hardness to a certain extent. The elastic modulus also shows a trend similar to the hardness with the increase of the bias voltage, that is, it first increases and then decreases. Furthermore, compared with the hardness of 1.7 GPa and elastic modulus of 86.2 GPa for the ZL109 alloy, the hardness and elastic modulus of the coating are significantly higher. This indicates that TiAlN as a protective coating has great advantages in improving the surface mechanical properties of ZL109 alloy.

3.4 Tribological properties of TiAlN coating

Figure 10 shows the variation of the coating coefficient of friction (COF) with sliding time. It can be observed that the friction curves of the coatings include two distinct stages: the running-in period and the stable period. During the running-in period, the initial COF shows a low value of about 0.11, which is attributed to the small actual contact area with the counterpart caused by droplets and contaminants. As the sliding time increases to about 110 s, due to the increase in the contact area and the appearance of furrows and abrasive particles in the wear track, the COF rapidly increases to a maximum value of about 0.63. When the sliding time is further increased, more abrasive particles may act as isolation and load-bearing sites, reducing the COF slightly to around 0.5. Subsequently, as the number of abrasive particles entering and leaving the wear track surface reaches a dynamic balance, the COF remains stable with slight fluctuations during the remaining time. In the stable period, TiAlN coatings with different bias voltages exhibit similar COFs, 0.44−0.49, which is significantly lower than 0.6−0.8 in Ref. [44].

In order to identify the wear mechanism of the coating, the morphology of the wear track is characterized by CLSM, as shown in Fig. 11. A large number of ploughs and wear particles can be observed in the wear track. Also, small amounts of black debris are distributed around the edges of the wear track. The appearance of ploughs and wear

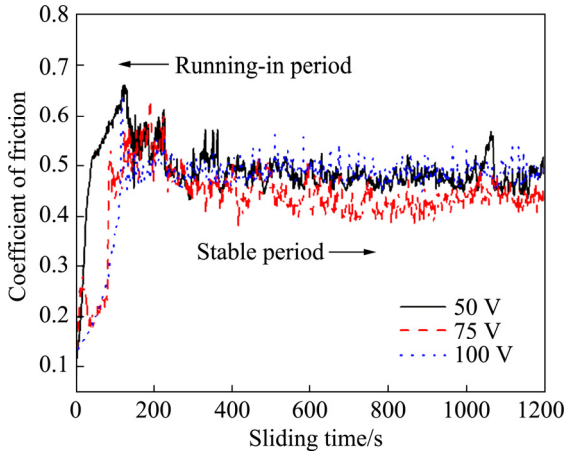

Fig. 10 Friction curves of TiAlN coating as function of sliding time

debris indicates signs of abrasive wear and adhesive wear, respectively [14,44]. Therefore, it can be considered that the wear mechanism of the coating is severe abrasive wear and slight adhesive wear. Furthermore, as the bias voltage increases from 50 to 75 V, the width of the wear track decreases from 625.4 to 514.5 μm, indicating that the TiAlN coating with a bias voltage of 75 V has better wear resistance. However, the width of the wear track increases to 685.9 μm when the bias voltage is further increased to 100 V.

Figure 12 shows the wear rate, H/E and H^3/E^2 values of TiAlN coatings with different bias voltages, where H is the hardness and E is the elastic modulus. As the bias voltage increases from 50 to 100 V, the wear rate first decreases and then increases. The H/E and H^3/E^2 exhibit the same change trend, that is, first increase and then decrease, which is the opposite to the change of wear rate. High H/E value is beneficial to reducing the ploughing effect and obtaining a low coefficient of friction [45]. When the bias voltage is 75 V, H/E and H^3/E^2 exhibit maximum values of 0.132 and 0.439 GPa, respectively. Meanwhile, wear rate of the coating is the lowest, about 4.44×10^{-5} mm^3/(N·m), lower than 1.8×10^{-4} mm^3/(N·m) for TiAlN/Ta multilayer coatings reported in the literature [46]. H/E and H^3/E^2 of hard coatings are related to resistance to cracking and plastic deformation, which can be used to predict wear resistance [29]. In this work, all TiAlN coatings show high toughness (H/E, ~0.13) and excellent resistance to plastic deformation (H^3/E^2, ~0.40 GPa). Higher hardness means higher load-carrying capacity, which helps reduce the actual contact area with the friction counterpart in the test, thereby

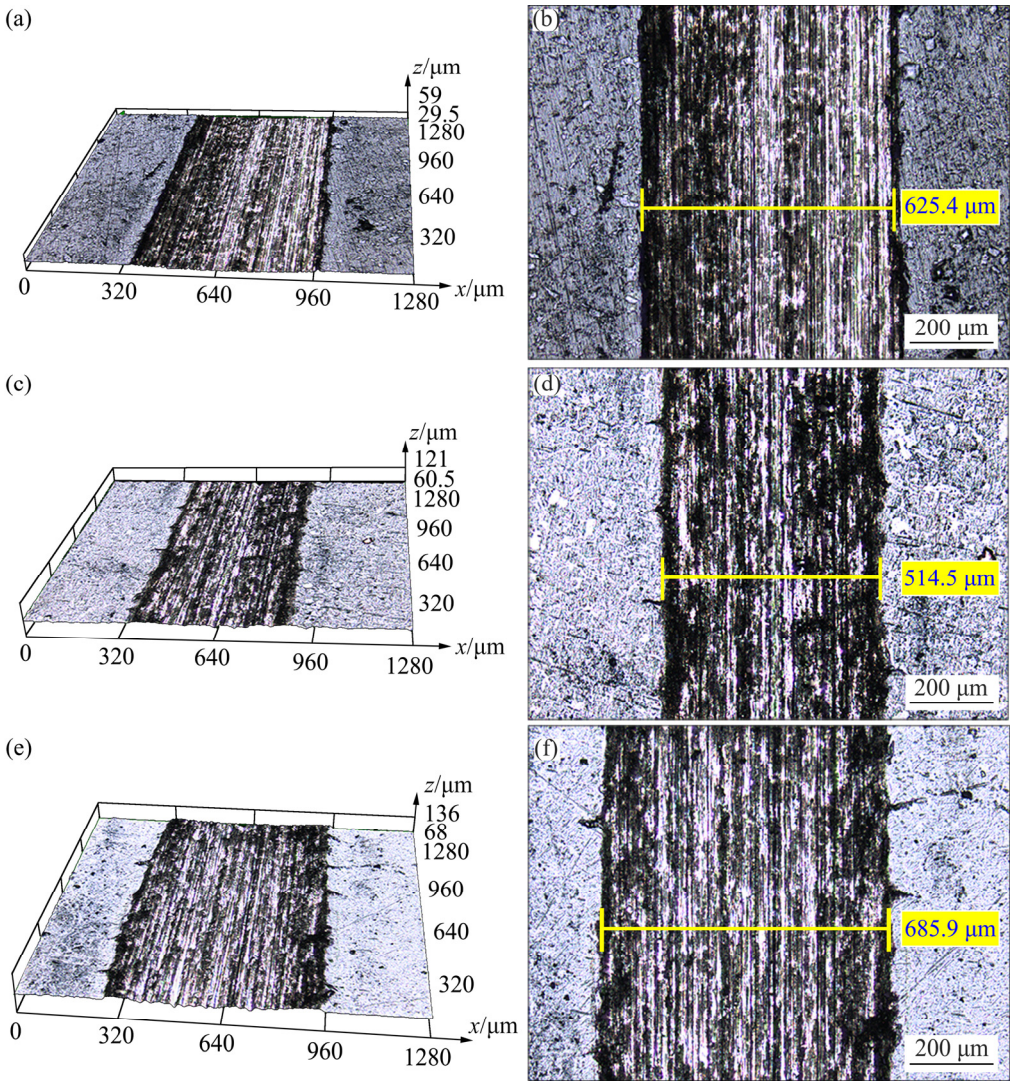

Fig. 11 Wear track morphologies of TiAlN coatings deposited at different bias voltages: (a, b) 50 V; (c, d) 75 V; (e, f) 100 V

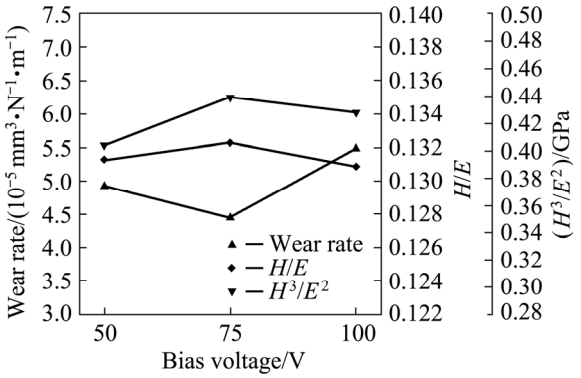

Fig. 12 Wear rate, H/E and H^3/E^2 of TiAlN coatings deposited at different bias voltages

reducing the amount of wear. In addition, high hardness is beneficial to reducing plastic yielding, while lower elastic modulus can reduce the maximum contact pressure by allowing a given load to be distributed over a larger area. MUSIL et al [47] pointed out that satisfying H/E>0.1 and H^3/E^2 in the range of 0.15−0.3 GPa are important conditions for well lubrication and good wear resistance. Furthermore, compared with the substrate wear rate of about 3.08×10^{-4} mm^3/(N·m), the wear rate of the TiAlN-coated ZL109 alloy has been reduced to one-seventh, indicating a significant improvement in wear resistance.

4 Conclusions

(1) The TiAlN multilayer coating composed of the TiAl transition layer and TiAlN layer prepared via filtered cathodic vacuum arc technology shows a uniform and dense surface and good interfacial bonding. Bias voltage has an important influence on the composition, structure and properties of the coating.

(2) As the bias voltage increases from 50 to 100 V, the Ti content in the coating is increased from 22.13 to 23.18 at.%, while the Al content decreases from 24.65 to 22.68 at.%. The coating exhibits a multi-phase structure with fcc TiAlN phase as the main phase and a small amount of TiN and AlN phases. When the bias voltage is increased from 50 to 75 V, the orientation of TiAlN changes from (200) to (111) due to the increase of atomic mobility and lattice distortion. However, as the bias voltage is further increased to 100 V, the intensity of TiAlN (111) decreases slightly, and the (220) diffraction peak occurs.

(3) The adhesion strength, hardness and elastic modulus of the coating are improved with increasing bias voltage from 50 to 75 V. Due to the annealing and sputtering effects caused by the high bias voltage, the adhesion strength and hardness of the coating with a bias voltage of 100 V are slightly reduced. The TiAlN coating deposited at a bias voltage of 75 V shows the best wear resistance due to the highest hardness (~30.3 GPa), high toughness (H/E=0.132) and good resistance to plastic deformation (H^3/E^2=0.439 GPa). TiAlN as a protective coating can significantly enhance the surface properties of ZL109 alloy.

Acknowledgments

This study was jointly supported by Hunan Provincial Natural Science Foundation, China (No. 2021JJ30646), Educational Commission of Hunan Province, China (No. 20B579), the National Natural Science Foundation of China (Nos. 51701172, 12027813), and Innovation Team of Hunan Province, China (No. 2018RS3091).

References

[1] DURSUN T, SOUTIS C. Recent developments in advanced aircraft aluminium alloys [J]. Materials & Design, 2014, 56: 862−871.

[2] RAGAB K A, BOUAICHA A, BOUAZARA M. Development of fatigue analytical model of automotive dynamic parts made of semi-solid aluminum alloys [J]. Transactions of Nonferrous Metals Society of China, 2018, 28(6): 1226−1232.

[3] LIU X F, WANG Y, LIU W H. Finite element analysis of thermo-mechanical conditions inside the piston of a diesel engine [J]. Applied Thermal Engineering. 2017, 119(5): 312−318.

[4] YAO Zhi-min, HU Kun-sheng, LI Rong. Enhanced high-temperature thermal fatigue property of aluminum alloy piston with Nano PYSZ thermal barrier coatings [J]. Journal of Alloys and Compounds, 2019, 790(25): 466−479.

[5] RODRÍGUEZ-BARACALDO R, BENITO J A, PUCHI-CABRERA E S, STAIA M H. High temperature wear resistance of (TiAl)N PVD coating on untreated and gas nitrided AISI H13 steel with different heat treatments [J]. Wear, 2007, 262(3/4): 380−389.

[6] ZHAO Hui, WANG Xiao-hui, LIU Qiu-lei, CHEN Li-jia, LIU Zheng. Structure and wear resistance of TiN and TiAlN coatings on AZ91 alloy deposited by multi-arc ion plating [J]. Transactions of Nonferrous Metals Society of China, 2010, 20(S2): s679−s682.

[7] WU S K, LIN H C, LIU P L. An investigation of unbalanced-magnetron sputtered TiAlN films on SKH51 high-speed steel [J]. Surface and Coatings Technology, 2000, 124: 97−103.

[8] ZHANG G P, GAO G J, WANG X Q, LV G H, ZHOU L,

CHEN H, PANG H, YANG S Z. Influence of pulsed substrate bias on the structure and properties of Ti–Al–N films deposited by cathodic vacuum arc [J]. Applied Surface Science, 2012, 258(19): 7274−7279.

[9] HEO J Y, CHO S H, JE T J, KIM K H, LEE H W, KANG M C. Effects of honing treatment on AIP-TiN and TiAlN coated end-mill for high speed machining [J]. Transactions of Nonferrous Metals Society of China, 2011, 21(S1): s83−s87.

[10] BADINI C, DEAMBROSIS S M, OSTROVSKAYA O, ZIN V, PADOVANO E, MIORIN E, CASTELLINO M, BIAMINO S. Cyclic oxidation in burner rig of TiAlN coating deposited on Ti−48Al−2Cr−2Nb by reactive HiPIMS [J]. Ceramics International, 2017, 43(1): 5417−5426.

[11] SHUAI Jin-tao, ZUO Xiao, WANG Zhenyu, SUN Li-li, CHEN Ren-de, WANG Li, WANG Ai-ying, KE Pei-ling. Erosion behavior and failure mechanism of Ti/TiAlN multilayer coatings eroded by silica sand and glass beads [J]. Journal of Materials Science & Technology, 2021, 80: 179−190.

[12] SHUGUROV A R, KAZACHENOK M S. Mechanical properties and tribological behavior of magnetron sputtered TiAlN/TiAl multilayer coatings [J]. Surface and Coatings Technology, 2018, 353: 254−262.

[13] WEI Yong-qiang, LI Chun-wei, GONG Chun-zhi, TIAN Xiu-bo, YANG Shi-qin. Microstructure and mechanical properties of TiN/TiAlN multilayer coatings deposited by arc ion plating with separate targets [J]. Transactions of Nonferrous Metals Society of China, 2011, 21(5): 1068−1073.

[14] YAN Hong-jun, TIAN Qin-ye, GAO De-wen, YANG Fei-fei. Microstructure and properties of TiAlN/AlN multilayers with different modulation periods [J]. Surface and Coatings Technology, 2019, 363: 61−65.

[15] LEE J K, YANG G S. Preparation of TiAlN/ZrN and TiCrN/ZrN multilayers by RF magnetron sputtering [J]. Transactions of Nonferrous Metals Society of China, 2009, 19(4): 795−799.

[16] ZHAO Sheng-sheng, DU Hao, ZHENG Jing-di, YANG Ying, WANG Wei, GONG Jun, SUN Chao. Deposition of thick TiAlN coatings on 2024 Al/SiC_p substrate by Arc ion plating [J]. Surface and Coatings Technology, 2008, 202: 5170−5174.

[17] OSTROVSKAYA O, BADINI C, DEAMBROSIS S M, MIORIN E, BIAMINO S, PADOVANO E. Protection from oxidation of second and third generation TiAl intermetallic alloys by magnetron sputtering deposition of a TiAl/TiAlN coating [J]. Materials & Design, 2021, 208: 109905.

[18] VOGLI E, TILLMANN W, SELVADURAI-LASSL U, FISCHER G, HERPER J. Influence of Ti/TiAlN-multilayer designs on their residual stresses and mechanical properties [J]. Applied Surface Science, 2011, 257(20): 8550−8557.

[19] BROWN I G, GODECHOT X. Vacuum arc ion charge-state distributions [J]. IEEE Transactions on Plasma Science, 1991, 19(5): 713−717.

[20] CAI Fei, CHEN Mo-han, LI Ming-xi, ZHANG Shi-hong. Influence of negative bias voltage on microstructure and property of Al−Ti−N films deposited by multi-arc ion plating [J]. Ceramics International, 2017, 43(4): 3774−3783.

[21] WEI Yong-qiang, ZONG Xiao-ya, JIANG Zhi-qiang, TIAN Xiu-bo. Characterization and mechanical properties of TiN/TiAlN multilayer coatings with different modulation periods [J]. The International Journal of Advanced Manufacturing Technology, 2018, 96: 1677−1683.

[22] MIENTUS R, ELLMER K. Reactive DC magnetron sputtering of elemental targets in Ar/N_2 mixtures: Relation between the discharge characteristics and the heat of formation of the corresponding nitrides [J]. Surface and Coatings Technology, 1999, 116/117/118/119: 1093−1101.

[23] WANG C F, OU S F, CHIOU S Y. Microstructures of TiN, TiAlN and TiAlVN coatings on AISI M2 steel deposited by magnetron reactive sputtering [J]. Transactions of Nonferrous Metals Society of China, 2014, 24(8): 2559−2565.

[24] WANG Li-jun, WANG Meng-chao, CHEN Hui. Corrosion mechanism investigation of TiAlN/CrN superlattice coating by multi-arc ion plating in 3.5 wt.% NaCl solution [J]. Surface and Coatings Technology, 2020, 391: 125660.

[25] DÍAZ B, HÄRKÖNEN E, ŚWIATOWSKA, MAURICE V, SEYEUX A, MARCUS P, RITALA M. Low-temperature atomic layer deposition of Al_2O_3 thin coatings for corrosion protection of steel: Surface and electrochemical analysis [J]. Corrosion Science, 2011, 53(6): 2168−2175.

[26] ZHANG Guo-jun, WANG Tao, CHEN Hai-lin. Microstructure, mechanical and tribological properties of TiN/Mo_2N nano-multilayer films deposited by magnetron sputtering [J]. Surface and Coatings Technology, 2015, 261: 156−160.

[27] LI Guo-jian, LÜ Wen-zhang, LIU Shi-ying, LI Chao, ZHOU Yao-yao, WANG Qiang. Multilayer-growth of TiAlN/WS self-lubricating composite coatings with high adhesion and their cutting performance on titanium alloy [J]. Composites Part B: Engineering, 2021, 211: 108620.

[28] SATO K, ICHIMIYA N, KONDO A, TANAKA Y. Microstructure and mechanical properties of cathodic arc ion-plated (Al,Ti)N coatings [J]. Surface and Coatings Technology, 2003, 163/164: 135−143.

[29] ZHAO Biao-chun, ZHAO Xiao-xiao, LIN Liang-liang, ZOU Ling-li. Effect of bias voltage on mechanical properties, milling performance and thermal crack propagation of cathodic arc ion-plated TiAlN coatings [J]. Thin Solid Films, 2020, 708: 138116.

[30] WIESING M, DELOSARCOS T, GEBHARD M, DEVI A, GRUNDMEIER G. Analysis of dispersive interactions at polymer/TiAlN interfaces by means of dynamic force spectroscopy [J]. Physical Chemistry Chemical Physics, 2018, 20(1): 180−190.

[31] KUMAR DINESH D, RANI R, KUMAR N, PANDA K, KIRUBAHARAN KAMALAN A M, KUPPUSAMI P, BASKARAN R. Tribochemistry of TaN, TiAlN and TaAlN coatings under ambient atmosphere and high-vacuum sliding conditions [J]. Applied Surface Science, 2020, 499: 143989.

[32] YI Pei-yun, PENG Lin-fa, HUANG Jia-qiang. Multilayered TiAlN films on Ti6Al4V alloy for biomedical applications by closed field unbalanced magnetron sputter ion plating process [J]. Materials Science and Engineering C: Materials for Biological Applications, 2016, 59: 669−676.

[33] ESGUERRA-ARCE A, ESGUERRA-ARCE J, YATE L, AMAYA C, COY L E, AGUILAR Y, GUTIÉRREZ O,

MOYA S. Influence of the Al content on the in vitro bioactivity and biocompatibility of PVD $Ti_{1-x}Al_xN$ coatings for orthopaedic applications [J]. RSC Advances, 2016, 6(65): 60756−60764.

[34] SHUM P W, ZHOU Z F, LI K Y, SHEN Y G. XPS, AFM and nanoindentation studies of $Ti_{1-x}Al_xN$ films synthesized by reactive unbalanced magnetron sputtering [J]. Materials Science and Engineering B, 2003, 100(2): 204−213.

[35] CHEN J T, WANG J, ZHANG F, ZHANG G A, FAN X Y, WU Z G, YAN P X. Characterization and temperature controlling property of TiAlN coatings deposited by reactive magnetron co-sputtering [J]. Journal of Alloys and Compounds, 2009, 472(1/2): 91−96.

[36] RIZZO A, MIRENGHI L, MASSARO M, GALIETTI U, CAPODIECI L, TERZI R, TAPFER L, VALERINI D. Improved properties of TiAlN coatings through the multilayer structure [J]. Surface and Coatings Technology, 2013, 235: 475−483.

[37] ANANTHAKUMAR R, SUBRAMANIAN B, KOBAYASHI A, JAYACHANDRAN M. Electrochemical corrosion and materials properties of reactively sputtered TiN/TiAlN multilayer coatings [J]. Ceramics International, 2012, 38(1): 477−485.

[38] WANG Zhen-yu, LIU Jing-zhou, WANG Li, LI Xiao-wei, KE Pei-ling, WANG Ai-ying. Dense and high-stability Ti2AlN MAX phase coatings prepared by the combined cathodic arc/sputter technique [J]. Applied Surface Science, 2017, 396: 1435−1442.

[39] KEIDAR M, BEILIS I I, BOXMAN R L, GOIDSMITH S. Nonstationary macroparticle charging in an arc plasma jet [J]. IEEE Transactions on Plasma Science, 1995, 23(6): 902−908.

[40] LIN C K, HSU C H, CHENG Y H, OU K L, LEE S L. A study on the corrosion and erosion behavior of electroless nickel and TiAlN/ZrN duplex coatings on ductile iron [J]. Applied Surface Science, 2015, 324: 13−19.

[41] CAI J B, WANG X L, BAI W Q, ZHAO X Y, WANG T Q, TU J P. Bias-graded deposition and tribological properties of Ti-contained *a*-C gradient composite film on Ti6Al4V alloy [J]. Applied Surface Science, 2013, 279: 450−457.

[42] RAFAJA D, KLEMM V, SCHREIBER G, KNAPP M, KUŽEL R. Interference phenomena observed by X-ray diffraction in nanocrystalline thin films [J]. Journal of Applied Crystallography, 2004, 37(4): 613−620.

[43] WÜSTEFELD C, RAFAJA D, KLEMM V, MICHOTTE C, KATHREIN M. Effect of the aluminium content and the bias voltage on the microstructure formation in $Ti_{1-x}Al_xN$ protective coatings grown by cathodic arc evaporation [J]. Surface and Coatings Technology, 2010, 205: 1345−1349.

[44] XU Xing, SU Feng-hua, LI Zhu-jun. Tribological properties of nanostructured TiAlN/W2N multilayer coating produced by PVD [J]. Wear, 2019, 430/431: 67−75.

[45] SUN P L, HSU C H, LIU S H, SU C Y, LIN C K. Analysis on microstructure and characteristics of TiAlN/CrN nano-multilayer films deposited by cathodic arc deposition [J]. Thin Solid Films, 2010, 518(24): 7519−7522.

[46] CONTRERAS ROMERO E, HURTADO MACÍAS A, MÉNDEZ NONELL J, SOLÍS CANTO O, GÓMEZ BOTERO M. Mechanical and tribological properties of nanostructured TiAlN/TaN coatings deposited by DC magnetron sputtering [J]. Surface and Coatings Technology, 2019, 378: 124941.

[47] MUSIL J, NOVÁK P, ČERSTVÝ R, SOUKUP Z. Tribological and mechanical properties of nanocrystalline-TiC/*a*-C nanocomposite thin films [J]. Journal of Vacuum Science & Technology A, 2010, 28(2): 244−249.

偏压对 TiAlN 涂层微观结构、力学和摩擦学性能的影响

曹红帅[1,2]，刘福家[1,2]，李 好[1,2]，罗文忠[1,2]，齐福刚[1,2]，卢立伟[3]，赵 镍[1,2]，欧阳晓平[1,2]

1. 湘潭大学 材料科学与工程学院，湘潭 411105；
2. 湘潭大学 低维材料及应用技术教育部重点实验室，湘潭 411105；
3. 湖南科技大学 难加工材料高效精密加工湖南省重点实验室，湘潭 411201

摘 要：采用磁过滤真空阴极弧在 ZL109 合金表面沉积由 TiAl 和 TiAlN 组成的 TiAlN 多层涂层，并系统研究偏压对涂层微观结构和性能的影响。结果表明，涂层具有以 TiAlN 相为主的多相结构。随着偏压的增大，由于原子迁移率和晶格畸变的增加，TiAlN 择优取向由(200)晶面向(111)晶面转变。同时，涂层的硬度、弹性模量和附着力表现出相同的变化趋势，即先增大后减小。当偏压为 75 V 时，TiAlN 涂层具有最高的硬度(~30.3 GPa)、弹性模量(~229.1 GPa)、附着力(HF 2)和最低的磨损率(~4.44×10^{-5} $mm^3/(N\cdot m)$)。与未涂覆 ZL109 合金相比，TiAlN 涂层合金表面的力学和摩擦学性能得到有效提高。

关键词：TiAlN 涂层；磁过滤真空阴极弧；偏压；微观结构；力学性能；磨损

(Edited by Bing YANG)